Reports

Atomic Force Microscopy of Atomic-Scale Ledges and Etch Pits Formed During Dissolution of Quartz

A. J. GRATZ,* S. MANNE, P. K. HANSMA

The processes involved in the dissolution and growth of crystals are closely related. Atomic force microscopy (AFM) of faceted pits (called negative crystals) formed during quartz dissolution reveals subtle details of these underlying physical mechanisms for silicates. In imaging these surfaces, the AFM detected ledges <1 nanometer (nm) high that were spaced 10 to 90 nm apart. A dislocation pit, invisible to optical and scanning electron microscopy measurements and serving as a ledge source, was also imaged. These observations confirm the applicability of ledge-motion models to dissolution and growth of silicates; coupled with measurements of dissolution rate on facets, these methods provide a powerful tool for probing mineral surface kinetics.

A LARGE NUMBER OF INDUSTRIAL and natural processes involve the dissolution and growth of crystals from aqueous solutions. Crystals are synthetically grown for use as electronic components, gems, reagents, and pharmaceuticals, and are etched as part of routine materials evaluation. In nature, minerals form from some fluids only to be attacked by others, and the lithification of sediments depends on a variety of growth and dissolution steps. Silicates in particular are unique in their dual importance in manufacturing and in geologic studies.

The attempt to understand and quantify these diverse phenomena has led to a recent proliferation of dissolution rate studies on silicates. Traditionally, powders are used in measurements of dissolution in order to maximize surface area and thus the total rate of mass transfer. However, such measurements are hindered by the need to determine the surface area, the problem of surface area versus active site density, and the difficulties of preparation and reproducibility of particulates. More recently, Gratz *et al.* (*1*) developed the "negative crystal method" for measuring the dissolution rate of quartz in basic solution by observing the retreat velocity of nearly perfect crystal faces. In this approach, which is a modification of the methods of Hulett and Young (*2*) and Liepmann (*3*), the expansion of faceted depressions (negative crystals, Fig. 1) formed by the etching of surface microfractures is measured from optical micrographs. The dissolving surfaces are nearly crystallographic, so that the nature of surface sites is strongly constrained. In particular, the classical model of Burton, Cabrera, and Frank (*4*) (BCF model) and Hirth and Pound (*5*) suggests that such surfaces should be dominated by ledges whose motion controls dissolution rate.

As originally conceived, this theory was based on a "Kossel crystal," an idealized crystal surface composed of cubic structural units (Fig. 2). A smooth surface consisting of 5-bonded "in surface" units can grow or evaporate only with difficulty because of the energy barrier associated with increased surface area during nucleation of hillocks or pits. This energy barrier is circumvented by bulk defects, in particular dislocations, which create offsets on the surface that are perpetuated during growth or dissolution. Such offsets are manifest as monatomic steps (ledges). "In ledge" sites are 4-bonded, "kinks" in ledges are 3-bonded, and units "at" a ledge are 2-bonded. Movement of 1-bonded units to and from the ledges causes ledge motion. It was further shown that 1-bonded units would travel rapidly by surface diffusion and be preferentially removed from locations between ledges where the total number of bonds of an adatom is at a minimum.

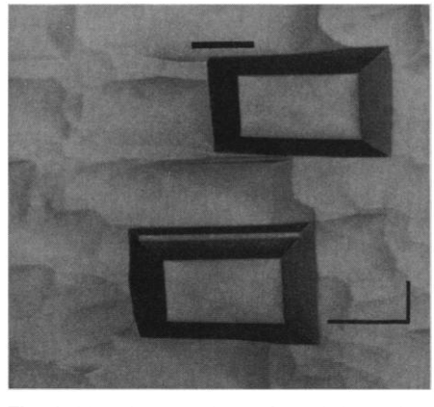

Fig. 1. Negative crystals are faceted depressions formed by removal of microfractures. The pair of quartz negative crystals shown here in a reflected light micrograph was formed during sequential dissolution experiments. Expansion of the negative crystals is then used to infer linear retreat rate of the constituent facets (the walls and floor). Scale bar = 25 μm; long axis is ⟨*c*⟩, short axis is ⟨*a*⟩.

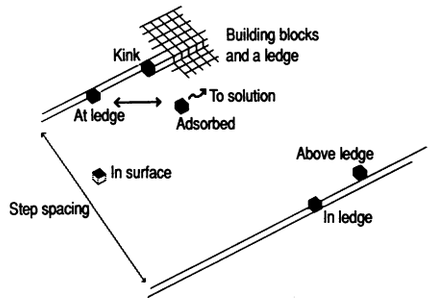

Fig. 2. A "Kossel crystal" made up of cubic structural units. The possible surface sites are labeled and discussed in the text. Note that the dissolution process consists of diffusion of cubic structural units from ledges onto the surfaces, where they are easily removed.

Application of this model to silicate dissolution creates a number of difficulties. First, silicates are polyatomic, and the coordination number of their constituent atoms is frequently less than six. For example, α-quartz consists of 4-coordinated silicon and 2-coordinated oxygen in a low-symmetry (trigonal) network structure; it may be envisioned as a network of SiO_4 tetrahedra with all corners shared. The fundamental reactive units are thus not atoms but tetrahedral groups. As Ernsberger noted (*6*), the nonreactive, unreconstructed prism and unit rhombohedra are "armored" by groups with three bonds connected to the bulk and one dangling oxygen (presumably hydrated in the presence of water); we call these "γ" groups (Fig. 3). In contrast, rapidly dissolving and growing directions such as the basal pinacoid (0001) expose exclusively groups with two bonds to the bulk, labeled here "β." Ledge units and one type of unit on a smooth surface are β groups, whereas a 1-bonded unit on a smooth face is an "α" group. Because γ groups are expected to be immobile, surface diffusion must occur by breaking an Si–O–Si bond of a β group to form an α group, pivoting about the remaining bond, then reattaching the group at a different site to form a new β group. (The alternative form of surface transport, de- and

A. J. Gratz, Department of Earth and Space Sciences, University of California, Los Angeles, CA 90024.
S. Manne and P. K. Hansma, Department of Physics, University of California, Santa Barbara, CA 93106.

*Present address: Department of Geosciences, Pennsylvania State University, University Park, PA 16802.

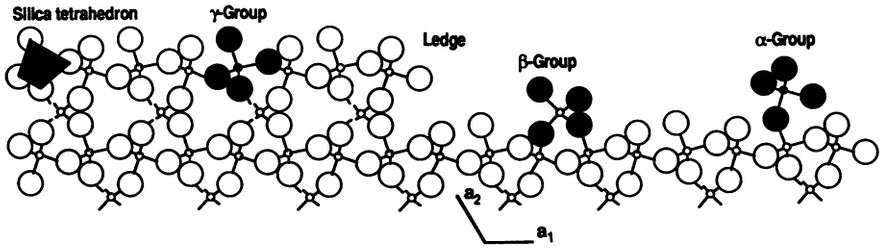

Fig. 3. The unreconstructed prism surface of quartz. Note that a smooth prism surface consists of a network of γ groups, which are resistant to attack. According to the BCF model, dissolution should proceed by migration of structural units (in this case, tetrahedra) from ledges onto smooth regions, followed by their removal into solution.

reattachment of groups, is unlikely in a highly undersaturated environment, although it cannot be ruled out.) "Kinks" in a quartz ledge, originally an important part of the BCF model, are not distinct from other ledge units.

In such a configuration, it is not immediately clear that the classical BCF model applies. It is therefore of interest to examine dissolution surfaces of quartz directly. In situ measurements of dissolution are precluded by the temperatures, pressures, and solution strengths needed to attain rapid material removal. However, the activation energy of quartz dissolution is sufficiently high (~90 kJ/mol) that very little change is likely to take place during cooling of a sample, so it suffices to make ex situ observations on a sample following a dissolution experiment. The samples studied were unit prisms $(10\bar{1}0)$ and rhombohedra $(10\bar{1}1)$ taken from optical-quality Brazilian quartz dissolved for 4 hours at 148° and 211°C in 0.01 *m* KOH solution. Details of the dissolution apparatus are given in Gratz *et al.* (*1*).

Observations were made with an atomic force microscope (AFM). Since its invention in 1986 (*7*), the AFM has been developed into a powerful new tool for the study of surface topography at subnanometer resolution (*8, 9*) and has been used to image atomic-scale structures of graphite (*10*), mica (*11*), NaCl (*12*), zeolites (*13*), and the clay minerals illite and montmorillonite (*14*). The AFM has also imaged large-scale chemical and biological processes such as corrosion (*15*) and fibrin polymerization (*11*) and can be operated under a variety of environments such as air, aqueous solutions (*11*), low temperature (*16*), and ultrahigh vacuum (*17*). The AFM used in this research has been described in detail elsewhere (*18–21*).

Prismatic (1010) floors of the negative crystals were studied in detail. We obtained best results working under ethanol, which seemed to clean the surface and permitted a smaller normal force during scans (*22*). The floors were found to be extremely smooth: high-magnification study of prismatic floors showed that they consisted of featureless regions separated by <1-nm-high ledges spaced at intervals of tens of nanometers, as predicted by the BCF theory. These were enhanced by subtracting out the baseline slope, revealing them as a series of ridges as shown in Fig. 4 for the sample etched at 211°C. The ledges were not always straight, but were crudely parallel to one another. Some very straight ledges were seen, along with a tendency toward ⟨*a*⟩ and ⟨*c*⟩ orientations [that is, parallel to crystal axes]. In any given region, ledges oriented normal to ⟨*c*⟩ were twice as widely spaced as those normal to ⟨*a*⟩. The presence of ledges produced average surface slopes of 2° to 3° relative to the flat regions between them.

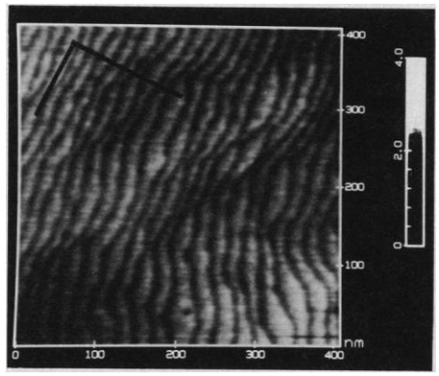

Fig. 4. An AFM gray-scale (unfiltered) image of a floor section of a quartz negative crystal scanned in air with $\leq 10^{-7}$ N applied force by the tip on the sample surface. With the background slope subtracted out for clarity, the terraced surface appears as a series of ridges. The image area is 410 nm by 410 nm, and the height difference between black (lowest) and white (highest) is 14.0 nm; the axes are ⟨*c*⟩ (long) and ⟨*a*⟩ short. The ledges are ~0.7 nm high with a spacing of 20 to 25 nm.

On negative crystal walls, convex intersections of the walls with the surrounding face serve as a source for ledges. On their floors, however, only intrinsic crystal defects or random plucking of γ groups can nucleate ledges. Observations of quartz etched in alkaline solution at low ionic strengths (<0.005 *m*) reveal the presence of small, optically visible pits at the outcrops of dislocations (*1*); at higher ionic strengths, however, no such pits are seen either optically or with high-resolution scanning electron microscopy, although a thermodynamic analysis suggests they should form (*23*). The resolution to this conflict lies in pit shape: we located several shallow-walled pits on surfaces that appeared smooth both to the optical and to the electron microscopes. The pit shown in Fig. 5 is an elongate amphitheater of atomic-scale steps with a central flat zone 50 nm by 100 nm and elongate in the ⟨*c*⟩ direction. The pit is quite shallow: surface slopes (formed by terracing) within the pit are very close to those in the surrounding area of the negative crystal, so that the pit is invisible to optical and electron microscopes. We note no spiraling as expected for a screw dislocation; it is probable this pit formed on an edge dislocation, since random plucking is unlikely to produce a deep pit.

The etch pit shape is explained by the mathematics of ledge motion. If the BCF model applies, surface diffusion is rapid and controls step spacing in the dissolution regime studied. A dislocation or other defect serves as a source of ledges, but ledge nucleation is suppressed until the preceding step reaches a critical distance. Strain effects on the dissolution energetics are small except within a few nanometers of the dislocation. Moreover, the rate-limiting step for dissolution can be shown to be detachment of α-groups (*23, 24*), and this process is unlikely to be strongly affected by elastic distortions in the quartz substrate. The etch pit formed in this regime should thus be a submicroscopic dish with slopes nearly identical to the background slopes, exactly as observed. The observed ellipticity of the quartz "etch dish" is indicative of a strong directionality to surface diffusion and can indeed be used to measure this directionality. Generation of optically visible etch pits is then associated with suppression of surface diffusion, decoupling the ledge nucleation, and motion processes. This process is discussed at length elsewhere (*23, 25*), as is the behavior of etch pits with hollow cores.

We observe groups of ledges both <0.5 nm and 0.7 to 1.0 nm in height. Mullins and Hirth (*26*) calculated that monomolecular ledges (0.425 nm high on the quartz prism face) should attract one another and that moving trains of monomolecular ledges are subject to an instability that causes them to group into pairs (0.85 nm high on the prism face). In this case, ledges higher than 0.4 nm may be pairs of monomolecular ledges with a spacing of less than ~2 nm, which were not easily resolved. Although these results appear to support Mullins and Hirth's theory, the present difficulties in measuring the

absolute height of atomic-scale features with the AFM make it impossible to be sure.

Measurements of atomic-scale topography open the door to highly detailed kinetic models. The dissolution rate of a face $R_{diss}(T)$ is the step height a times its velocity $v_{ledge}(T)$ divided by the step spacing $\lambda(T)$

$$R_{diss}(T) = a \cdot v_{ledge}(T)/\lambda(T) \quad (1)$$

where T is the temperature. For example, a step spacing of 20 nm for 0.83-nm-high steps (a double-step on the prism face) and a dissolution rate of 0.31 nm/s (*1*), both observed at 211°C, lead to a step velocity of ~8.5 nm/s. Once slopes are verified to be composed of steps and the step heights are measured, less time-consuming methods can be used to obtain slopes, and the slopes can be directly converted to step spacings.

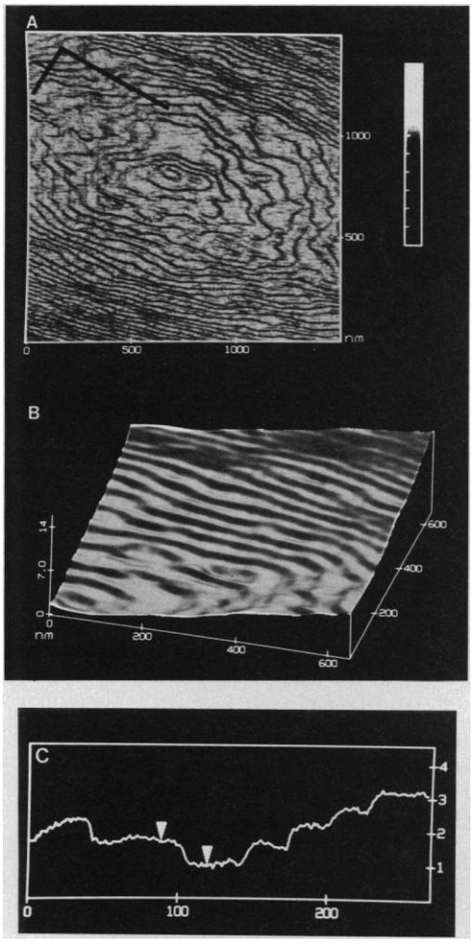

Fig. 5. A series of AFM images of a microscopic etch pit formed at 148°C in 0.01 *m* KOH, then scanned in ethanol with $\leq 10^{-8}$ N applied force. (**A**) View of an etch pit in "illumination mode," simulating a vertical light source reflecting off the pit surface to enhance edges between topographic levels. The image area is 1490 nm by 1490 nm, with a height difference of ~20 nm between the bottom of the pit and the highest point on the image. Again, a cross shows the ⟨*c*⟩ and ⟨*a*⟩ axes. (**B**) A surface plot of one quadrant of the etch pit. Image size is 650 nm by 650 nm by 14 nm. (**C**) Profile taken across the pit floor in the ⟨*a*⟩ direction. Note the wide (~30 nm), atomically flat regions separated by distinct ledges. The height between the cursors is 0.7 nm.

In order to refine the kinetic model of quartz dissolution, measurements of ledge spacing normal to the ⟨*c*⟩ direction were made on samples dissolved at 148° and 211°C in 0.01 *m* KOH. Spacings were quite variable and ranged from 15 to 40 nm at 148°C and from 20 to 25 nm at 211°C. [Interferometric study (*23, 24*), confirmed by this work, has suggested that steps may bunch at the perimeter of negative crystals, so we restricted our measurements to the same region of negative crystals, that is, midway between walls and centers.] Gratz *et al.* (*1, 23, 24*) have measured the dissolution rate for a wide range of conditions and found an apparent activation energy of 86.4 kJ/mol for dissolution. Since the ledge spacing shows no obvious change with temperature, the temperature dependence of dissolution rate must be due mostly to variations in ledge velocity. We can therefore use the average step spacing of ~20 nm with a simple Arrhenius rate formulation and replace Eq. 1 by

$$R_{diss}(T) \approx v_{ledge}(T)/24 \quad (2a)$$

$$v_{ledge}(T) \approx 17.8\ m/s \cdot \exp[(-86.4\ \text{kJ/mol})/RT] \quad (2b)$$

where R is the gas constant. Thus the combination of macroscopic kinetic measurements and AFM observations allows us to determine the energetics of fundamental processes, in this case the velocity of ledges.

We can make further generalizations about the behavior of quartz surfaces during dissolution. In contrast to evaporation, the surface of quartz will not roughen significantly with temperature during dissolution, at least until the melting point is approached. Sharp, crystallographic interfaces are to be expected both in dissolution and growth, and Eq. 2b can be used to find the ledge velocity as a function not only of temperature but also solution chemistry. Interferometric study (*23, 24*) shows the surface slope is also unaffected by changes in pH or salinity. According to the BCF model, moreover, the ledge spacing is expected to be independent of concentration (*4, 23, 24*), suggesting that the same spacing will apply for either growth or dissolution. The average ledge spacing can then only be affected by transport limitations (producing gradients in the attacking fluid) or by chemical poisoning of the surface.

This study represents a direct measurement of active dissolution sites for minerals. Our results are consistent with a BCF-type ledge-motion model for quartz dissolution. If more detailed models of the crystal surface are used, the energies and rate constants for the individual reactions determining ledge velocities and spacings can also be extracted; we have used our results to develop a detailed model specific to aqueous dissolution of quartz (*23, 24*). This model includes the participation of the solvent in surface diffusion and the low coordination of the atoms in the quartz structure. Probe microscopy holds the promise that rigorous microkinetic models can be constructed to describe growth and dissolution processes for a wide range of minerals and industrial materials. Such work should include further collaboration with kinetics experiments, observations of natural growth and dissolution surfaces of minerals, and attempts at in situ measurements of dissolution surfaces on more soluble minerals.

REFERENCES AND NOTES

1. A. J. Gratz, P. Bird, G. B. Quiro, *Geochim. Cosmochim. Acta* **54**, 2911 (1990).
2. L. D. J. Hulett and F. W. J. Young, *J. Phys. Chem. Solids* **26**, 1287 (1964).
3. M. J. Liepmann, thesis, University of California, Los Angeles (1985).
4. W. K. Burton, N. Cabrera, F. C. Frank, *Philos. Trans. R. Soc. London. Ser. A* **243**, 299 (1951).
5. J. P. Hirth and G. M. Pound, *J. Chem. Phys.* **26**, 1216 (1957).
6. F. M. Ernsberger, *J. Phys. Chem. Solids* **13**, 347 (1960).
7. G. Binnig, C. F. Quate, Ch. Gerber, *Phys. Rev. Lett.* **12**, 930 (1986).
8. K. Wickramasinghe, *Sci. Am.* **260**, 90 (October 1989).
9. D. Rugar and P. K. Hansma, *Phys. Today* **43**, 23 (October 1990).
10. G. Binnig, Ch. Gerber, E. Stoll, C. F. Quate, *Europhys. Lett.* **3**, 1281 (1987).
11. B. Drake *et al.*, *Science* **243**, 1586 (1989).
12. G. Meyer and N. M. Amer, *Appl. Phys. Lett.* **58**, 2100 (1990).
13. A. L. Weisenhorn *et al.*, *Science* **247**, 1330 (1990).
14. H. Hartman *et al.*, *Clays Clay Miner.* **38**, 337 (1990).
15. S. Alexander *et al.*, *J. Appl. Phys.* **65**, 164 (1989).
16. M. D. Kirk, T. R. Albrecht, C. F. Quate, *Rev. Sci. Instrum.* **59**, 833 (1988).
17. G. Meyer and N. M. Amer, *Appl. Phys. Lett.* **53**, 1045 (1988).
18. The apparatus is described in (*10*) and (*15*). It uses a microfabricated silicon nitride cantilever (*19*) combined with an optical lever detection technique (*17*). A 5- to 10-μm tip [either glued-on diamond or integrated pyramidal tip (*20*)] attached to the cantilever (length 100 μm, spring constant 0.6 N/m] is gently brought into contact with the sample surface. The sample is then raster-scanned with the use of an *xyz* piezoelectric translator, and the resulting deflection of the cantilever is measured by the deflection of a laser beam reflected off the back of the cantilever into a two-segment photodiode. Feedback electronics (*21*) keep this deflection constant by translating the sample along the *z*-axis as it is raster-scanned. This *z*-axis piezo translation is then read in as the height of the surface feature. The AFM can produce a complete image in a few seconds.
19. T. R. Albrecht and C. F. Quate, *J. Vac. Sci. Technol. A* **6**, 271 (1988).
20. Park Scientific Instruments, 476 Ellis Street, Mountain View, CA 94043.
21. Digital Instruments, Inc., 6780 Cortona Drive, Santa Barbara, CA 93117.

22. A. L. Wiesenhorn, P. K. Hansma, T. R. Albrecht, C. F. Quate, *Appl. Phys. Lett.* **54**, 2651 (1989).
23. A. J. Gratz, thesis, University of California, Los Angeles (1990).
24. _____ and P. Bird, unpublished results.
25. _____, E. Nolan, D. W. Coffee, in preparation.
26. W. W. Mullins and J. P. Hirth, *J. Phys. Chem. Solids* **24**, 1391 (1963).
27. We thank V. Elings, J. Massie, and others at Digital Instruments for Nanoscope II feedback electronics and for their assistance in our research, T. R. Albrecht and C. F. Quate for microfabricated cantilevers, P. Bird for valuable discussions and comments, C. B. Prater for illuminating suggestions on image processing, G. Kelderman for technical support, and E. Martzen for secretarial support. Supported by NASA under fellowship NGT-50228 (A.J.G.); by the donors of the Petroleum Research Fund under grant 19762-AC2, administered by the American Chemical Society (A.J.G.); by the National Science Foundation–Solid State Physics grant DMR89-17164 (S.M. and P.K.H.); by the Office of Naval Research (P.K.H.); and by a fellowship from the AT&T Foundation (S.M.).

24 September 1990; accepted 28 December 1990

Fluid Dynamics in Suspension-Feeding Blackfish

S. LAURIE SANDERSON,* JOSEPH J. CECH, JR., MARK R. PATTERSON

Measurements of flow patterns and water velocities inside the oral cavity of blackfish (*Orthodon microlepidotus*), made with a fiberoptic endoscope and thermistor flow probe, revealed that gill-arch structures act in blackfish as barriers that direct particle-laden water to the mucus-covered roof of the oral cavity, where particles are retained. Gill-arch structures have previously been assumed to be the site of particle retention in suspension-feeding fishes. Water does not pass between these structures in blackfish, and they do not serve as filters that separate particles from the water. These results emphasize the importance of directly assessing flow velocity and direction inside the oral cavity of vertebrate suspension feeders, particularly at the level of the filtering elements.

SUSPENSION-FEEDING FISHES FILTER large volumes of water past their feeding apparatus to capture minute planktonic prey. They belong to at least 12 families in nine orders (*1*) and make up approximately one-third of the world fish catch (*2*). Despite the ecological and economic importance of these fishes, hypotheses about mechanisms of particle entrapment inside their mouths have rarely been tested, and there have been no direct observations of particle retention. Most workers have assumed that rows of cartilaginous protuberances on the gill arches (for example, gill rakers, branchiospinules) act as the filter in suspension-feeding fishes (*3*). These structures may operate as a sieve, retaining particles larger than the pore size of the mesh (*4*). If the gill-arch structures have a sticky mucus coating, particles small enough to pass between the mesh may be trapped by direct interception, inertial impaction, gravitational deposition, or electrostatic entrapment (*5*). By developing a quantitative experimental approach, we have documented an unexpected mechanism of fish suspension feeding. The techniques we used for flow visualization and measurement can be adapted to study the function of internal feeding structures in a diversity of animals, including suspension-feeding birds and bivalves.

Like other suspension-feeding species in the family Cyprinidae, blackfish (*Orthodon microlepidotus*) use a series of suctions to engulf water in a pulsatile fashion. It is thought that particles captured on gill rakers are then transported by water currents to the esophagus during a processing phase (*6*). We obtained images of particle movements and measured water velocities inside the mouths of three adult blackfish [32 to 33 cm standard length (*7*)] using a fiberoptic endoscope and thermistor flow probe (*8*) threaded through a cannula implanted in the hyomandibula or neurocranium. The unrestrained fish fed freely on a mixture of dead brine shrimp adults (4 mm long) or brine shrimp nauplii (400 to 500 μm long), hydrated brine shrimp cysts (250 μm across), and polystyrene microspheres (40 to 80 μm across).

By inserting the tips of the endoscope and thermistor less than 1.5 mm into the oral cavity through the hyomandibula cannula, we positioned the instruments above the channel between the lateral and medial rows of rakers on the ventral region (ceratobranchial) of gill arch I (Fig. 1, location B). Insertion through the neurocranium provided access to the ceratobranchial of gill arch II (Fig. 1, location C). Videotapes of the endoscopic images confirmed that particles were not entrained by any eddies around the instrument tips. Videotaped sequences were selected at random for detailed analysis.

While the fish were feeding, only 3 of 228 particles that entered the field of view (3 to 4 mm in diameter) were actually retained by the gill rakers (Fig. 2, left); the remainder of the particles traveled across the field of view in the channel between the rows of rakers. In all, 84% of the particles (n = 168) were carried dorsally toward the roof of the oral cavity, whereas 16% were transported ventrally toward the floor. Almost all particles

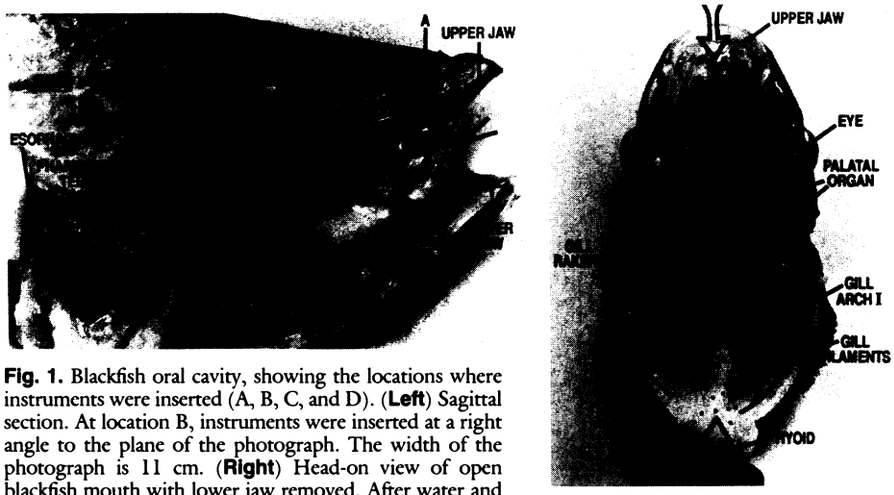

Fig. 1. Blackfish oral cavity, showing the locations where instruments were inserted (A, B, C, and D). (**Left**) Sagittal section. At location B, instruments were inserted at a right angle to the plane of the photograph. The width of the photograph is 11 cm. (**Right**) Head-on view of open blackfish mouth with lower jaw removed. After water and particles entered the mouth (open arrows), particles (dots) were observed to travel (solid arrows) along gill arches and palatal organ. Arrows at left of figure indicate that water exiting between the ventral regions (ceratobranchials) of the gill arches is not filtered. Filtered water exits between the dorsal regions (epibranchials) of the gill arches (not visible). The maximum width of the head is 5 cm. [Left photograph by L. Matteson; right photograph by L. Matteson and M. Massingill]

S. L. Sanderson and J. J. Cech, Jr., Department of Wildlife and Fisheries Biology, University of California, Davis, CA 95616.
M. R. Patterson, Division of Environmental Studies, University of California, Davis, CA 95616.

*Present address: Institute of Theoretical Dynamics, University of California, Davis, CA 95616.